International Journal of Heat and Mass Transfer 90 (2015) 1214–1220

Contents lists available at ScienceDirect

International Journal of Heat and Mass Transfer

journal homepage: www.elsevier.com/locate/ijhmt

Technical Note

Convection in a horizontal fluid layer under an inclined temperature gradient with a negative vertical Rayleigh number

A.S. Ortiz-Pérez [a], L.A. Dávalos-Orozco [b,*]

[a] Plan Educativo de Ingeniero Aeroespacial, Facultad de Ingeniería, Universidad Autónoma de Baja California, Blvd. Benito Juárez S/N, Unidad Universitaria, Mexicali 21280, Baja California, Mexico
[b] Instituto de Investigaciones en Materiales, Departamento de Polímeros, Universidad Nacional Autónoma de México, Ciudad Universitaria, Circuito Exterior S/N, Delegación Coyoacán, 04510 México D. F., Mexico

ARTICLE INFO

Article history:
Received 8 January 2015
Received in revised form 14 July 2015
Accepted 14 July 2015
Available online 3 August 2015

Keywords:
Thermal convection
Inclined temperature gradient
Pattern formation
Hadley circulation
Atmospheric flows

ABSTRACT

In this paper natural convection is investigated under an inclined temperature gradient with a negative vertical component. This is translated into a negative vertical Rayleigh number R_V. This is important in applications when, for example, $R_V < 0$ is used to stabilize a liquid layer but a horizontal temperature gradient still persists. Interesting results are found from the numerical analysis of the linear equations. New codimension-two points, where the stationary and oscillatory convection modes compete to be the first unstable one, are found by increasing the magnitude of the negative R_V. Besides, the longitudinal stationary modes intersect again for $R_V < 0$. Calculations for seven magnitudes of the Prandtl number are presented in detail.

1. Introduction

The motion of a liquid due to buoyancy effects is the source of different problems when solidification of the material is the final goal of an industrial process. A method to avoid convective motions is to maintain the room at a very well controlled uniform temperature. If this is not possible, the motion can be suppressed if the system is cooled from below. This phenomenon occurs when a thermal inversion exists in the atmosphere. However, this method fails if a horizontal temperature gradient is imposed in addition to the cooling vertical temperature gradient. As found in nature, industry and in the laboratory, temperature gradients are not only in the vertical direction but appear inclined with respect to gravity. As will be shown presently, an inclined temperature gradient is able to destabilize a horizontal fluid layer even when it is cooled from below. Furthermore, it has the possibility of changing the first unstable modes of instability as well.

The case of a purely horizontal temperature gradient was investigated many years ago to explain phenomena in molten metals [1,2] and in the atmosphere (the so called Hadley circulation [3]). Some applications to the problem of crystal growth were made by Lappa [4]. Under the assumption of a small aspect ratio this problem has also been investigated by other authors like Kuo et al. [5], Kuo et al. [6] and Wang et al. [7], Laure [8] and Laure and Roux [9] and Hughes and Griffiths [10] (review of oceanographic applications). The nonlinear problems were investigated in [7,9,11] and experiments were performed in [12,13]. The effect of a vertical magnetic field was included by Baaziz et al. [14]. For a comprehensive review of this problem and others related with convection see [15,16].

Linear convection under a purely vertical temperature gradient is reviewed in Chandrasekhar [17]. As mentioned above, it is difficult to find a pure vertical or horizontal temperature gradient. Therefore, a number of papers are devoted to investigate the influence of an inclined temperature gradient on the stability of a horizontal fluid layer. This case was investigated by Weber [18], Sweet et al. [19], Bhattacharyya and Nadoor [20] and Weber [21]. These papers introduced simplifying assumptions in the calculations. Nield [22] is the first to make a more complete numerical calculation introducing a wider range of Prandtl numbers. The nonlinear energy method is used by Kaloni and Qiao [23] who pointed out the important result that the curves of Nield [22] should decrease when the horizontal Rayleigh number increases.

The two papers by Nield [22] and Kaloni and Qiao [23] were the motivation to make numerical calculations of the linear problem under an inclined temperature gradient in a wider range of the horizontal Rayleigh number and Prandtl number (see Ortiz-Pérez and Dávalos-Orozco [24,25]). Those papers present the

* Corresponding author.
E-mail address: ldavalos@unam.mx (L.A. Dávalos-Orozco).

http://dx.doi.org/10.1016/j.ijheatmasstransfer.2015.07.057
0017-9310/

Nomenclature

d	thickness of the layer
D/Dt	Lagrange operator
$D = d/dz$	symbol of z-derivative
g	acceleration of gravity
k	x-direction wavenumber
$\mathbf{k}$	vertical unit vector
l	y-direction wavenumber
L_{O1}	even longitudinal oscillatory mode
L_{O2}	odd longitudinal oscillatory mode
L_{S1}	even longitudinal stationary mode
L_{S2}	odd longitudinal stationary mode
Obo	oblique mode
p'	pressure perturbation
Pr	Prandtl number
R_V	vertical Rayleigh number
R_{VC}	vertical critical Rayleigh number
R_H	horizontal Rayleigh number
$T(x,z)$	main temperature profile
T'	nondimensional temperature
To	transversal oscillatory mode
Ts	transversal stationary mode
$\bar{u}' = (u', v', w')$	nondimensional velocity perturbation
$u(z)$	x-direction perturbation amplitude
$U(z)$	x-direction main flow
$V(z)$	y-direction main flow
$w(z)$	z-direction perturbation amplitude

Greek

α	wavenumber magnitude
α_C	critical wavenumber magnitude
α_T	coefficient of volumetric expansion
β_H	horizontal temperature gradient
ΔT	vertical temperature difference
θ	amplitude of temperature perturbation
κ	thermal diffusivity
ν	kinematic viscosity
ρ_0	reference density
σ	frequency of oscillation
σ_C	critical frequency of oscillation
ϕ	perturbation propagation angle
ϕ_C	perturbation critical propagation angle

competition among a variety of modes to be the first unstable one. In particular, codimension-two points, where the stationary and oscillatory modes compete to be the first unstable one, were found including those calculated for the new oblique oscillatory mode. The way to see how this occurs is by looking at the marginal curves. Let's say that the marginal curve of the stationary mode has a minimum (the critical) at some height of the vertical Rayleigh number and that the marginal curve of the oscillatory mode has a minimum at a lower height (that means that it is more unstable). When changing one of the parameters, in particular the horizontal Rayleigh number, the minimum of the stationary mode decreases and the minimum of the oscillatory mode increases in such a way that at some magnitude of the horizontal Rayleigh number both minima have the same magnitude in the vertical Rayleigh number (but different critical wavenumber). At this point, the codimension-two point, both modes compete to be the more unstable. All the calculations in [24,25] assume positive vertical Rayleigh numbers (heating from below). Here, the calculations are focused on natural convection under an inclined temperature gradient but under the assumption of a negative vertical Rayleigh number (cooling from below). As will be seen presently, these conditions will prove to be very fruitful and will lead to new interesting phenomena.

The next section presents the equations of motion for the description of the fluid flow and heat transfer of the system under investigation and reviews the numerical method used to solve the linear system of equations. The results of the numerical calculations are given in Section 3 along with a detailed analysis of the main temperature profile. The discussion is presented in Section 4.

2. Equations of motion

A schematic representation of the system under investigation is shown in Fig. 1. The difference with respect to previous work [24,25] is that here it is assumed that the temperature difference between the upper and lower solid walls satisfies $\Delta T < 0$. Gravity is perpendicular to the fluid layer in the negative direction of the z-axis. A horizontal temperature gradient of magnitude β_H is imposed in the x-direction. Here, the interest is on the stability of the flow in a middle region far from the lateral walls. Thus, the flow in the x-direction due to β_H has the form of a very large cell. The corresponding dimensional main velocity profile depends only on the z-coordinate as $\overline{U(z)}$.

The equations of motion and heat transfer are made non dimensional by means of the following quantities. The thickness of the layer d is used for distances, d^2/κ for time (κ is the thermal diffusivity), κ/d for velocity, $\rho_0\kappa\nu/d^2$ for pressure (ρ_0 is a reference density) and $\Delta T/R_V$ for temperature. Here the vertical Rayleigh number is defined as $R_V = g\alpha_T d^3\Delta T/\nu\kappa$ and the horizontal Rayleigh number is $R_H = R_V d\beta_H/\Delta T = g\alpha_T d^4\beta_H/\nu\kappa$. g is the acceleration of gravity and α_T is the coefficient of volumetric expansion. Hence, the non dimensional equations of motion, heat diffusion and mass conservation are, respectively:

$$Pr^{-1}\frac{D\bar{u}'}{Dt} = -\nabla p' + T'\mathbf{k} + \nabla^2\bar{u}' \tag{1}$$

$$\frac{DT'}{Dt} = \nabla^2 T' \tag{2}$$

$$\nabla\cdot\bar{u}' = 0 \tag{3}$$

where use is made of the Boussinesq approximation. Here, $\bar{u}' = (u', v', w')$ is the velocity vector, $\mathbf{k}$ is a vertical unit vector, p'

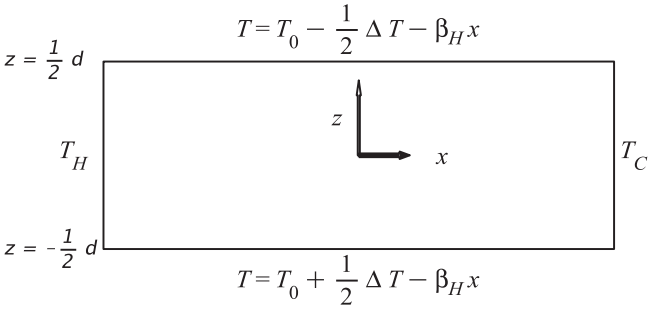

Fig. 1. Sketch of the system. The two solid walls are separated a distance d and have a negative temperature difference $\Delta T < 0$. The walls are also subjected to a horizontal temperature gradient of magnitude β_H in the x-direction. The lateral walls are assumed to be located very far from the region under investigation.

is the pressure, T' is the temperature and D/Dt is the Lagrange operator. The walls are located at $z = \pm 1/2$ and are assumed to be rigid and very good conductors. There, the velocity and temperature satisfy the conditions:

$$\bar{u}' = 0 \tag{4}$$

$$T' = \mp R_V/2 - R_H x \tag{5}$$

The solution of the main flow and temperature profiles in the region far from the lateral walls is obtained from the following three equations.

$$D^3 U(z) = -R_H \tag{6}$$

$$D^3 V(z) = 0 \tag{7}$$

$$D^2 T(x,z) = -R_H U(z) \tag{8}$$

where the operator D stands for d/dz. Note that the flow is closed and should satisfy the zero mass flux condition by making zero the integrals of the main velocity components in the range of z. The results are

$$U(z) = R_H\left(\frac{z}{24} - \frac{z^3}{6}\right) \tag{9}$$

$$V(z) = 0 \tag{10}$$

$$T(x,z) = R_H^2\left(\frac{7z}{5760} - \frac{z^3}{144} + \frac{z^5}{120}\right) - R_V z - R_H x \tag{11}$$

It is important to observe that the numerical calculations are done under the assumption $R_V < 0$. Thus, the main temperature profile differs from that of previous results [24,25] (see discussion below). This has important consequences on the stability, as will be shown presently. More general temperature profiles have been investigated by Lappa [26] and Andreev and Stepanova [27].

The system is subjected to linear perturbations [22,24,25] and the Eqs. (1)–(3) are transformed into the following.

$$[Pr(D^2 - \alpha^2) - i(kU - \sigma)](D^2 - \alpha^2)w + ikwD^2 U - Pr\alpha^2\theta = 0 \tag{12}$$

$$[(D^2 - \alpha^2) - i(kU - \sigma)]\theta + R_H u - wDT = 0 \tag{13}$$

$$[Pr(D^2 - \alpha^2) - i(kU - \sigma)](-\alpha^2 u + ikDw) + l^2 wDU = 0 \tag{14}$$

It is assumed that the dependent variables have the form $G(z)\exp[i(kx + ly - \sigma t)]$, where $G(z)$ represents the amplitude of any of the perturbations and k and l are the x and y-components of the wavenumber with magnitude $\alpha = \sqrt{k^2 + l^2}$. Therefore, $k = \alpha\cos\phi$ and $l = \alpha\sin\phi$, where ϕ is the angle of propagation of the perturbation. σ is a complex number whose real part is the frequency of oscillation of the perturbation and its imaginary part is the growth rate.

The amplitudes u and w are the x- and z-components of the velocity perturbation and θ is the temperature perturbation. They satisfy the boundary conditions for solid and very good heat conducting walls, that is, $w = Dw = u = \theta = 0$ at $z = \pm 1/2$.

The numerical Galerkin method [28,29] in this paper follows that of Hart [30] as used in [24,25]. The good convergence has already been verified and the number of expansion terms have been increased as needed. Due to the symmetries [24,25] found in Eqs. (12)–(14), numerical calculations are performed only for the angles ϕ between 0° and 90°.

3. Numerical results

The numerical calculations are focused on magnitudes of the Prandtl number where the results are not expected and are in contrast to the case of $R_V > 0$. In this way, the first calculations are for $Pr = 0.14$, which correspond to molten iron at 1870 °C [31]. Notice that in all the figures, the flow is stable in the region below the curves of criticality. As shown in Fig. 2 in a plot of R_{VC} vs R_H, the curve of the first longitudinal oscillatory mode L_{O1} intersects that of the transverse stationary mode T_S, point after which T_S becomes the first unstable one. Therefore, for $Pr = 0.14$ and $R_V < 0$ a new codimension-two point is found. Based on the results of Fig. 3 in [24] these two curves also have a codimension-two point for $R_V > 0$. If the data are presented in the form $(R_H, R_{VC}, \alpha_C, \sigma_C)$ the first codimension-two point [24] appears at (1661.00, 1425.83, 2.64, 0) for T_S and at (1661.00, 1425.83, 2.27, 12.31) for L_{O1}. The second new one appears at (3052.00, −2617.14, 2.44, 0) for T_S and at (3052.00, −2617.14, 1.75, 19.54) for L_{O1}. Notice the negative R_{VC}.

It is important to point out that this new codimension-two point discussed above, starts to appear very near to $Pr = 0.14$ as can be seen by the close distance between the two curves. The critical wavenumbers of both modes decrease with R_H while the critical frequency of oscillation of L_{O1} increases. Note that in this figure the first and second longitudinal modes L_{S1} and L_{S2} are not shown because they only appear for very large R_H when $R_{VC} < 0$ and never become the first unstable ones. Physically mode T_S and L_{S1} appear from natural convection with vertical temperature gradient. It is found [24] that T_S is the most unstable when shear flow increases with R_H and that L_{S1} first stabilizes. The increase of shear flow with R_H has stabilizing effects, until certain magnitudes, which work against buoyancy forces. This produces the first oscillatory longitudinal mode L_{O1} which now competes against T_S. However, the cooling from below returns the dominance to T_S. These two modes have a one cell structure [24].

The case of $Pr = 0.16$ is investigated in order to find out if these two modes T_S and L_{O1} behave in the same way increasing Pr slightly. For example, molten iron at 1830 °C [31] corresponds to $Pr = 0.16$. In fact it is shown that the two curves still meet at a codimension-two point but for a larger magnitude of negative R_V, as seen in Fig. 3. The full picture is as follows. The first codimension-two point for positive R_V appears for T_S at (1178.00,

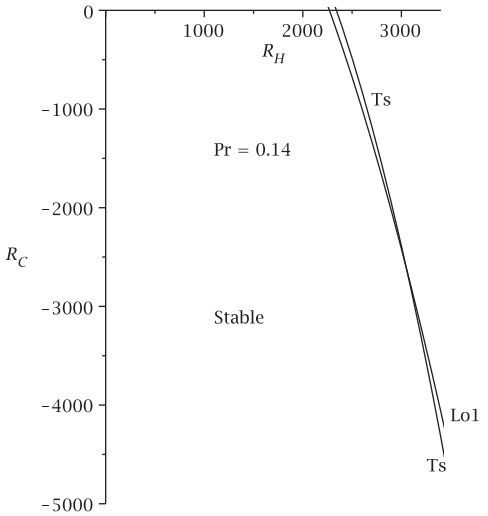

Fig. 2. Graphs of R_{VC} vs R_H for $Pr = 0.14$. New codimension-two point between Ts and L_{O1} for $R_V < 0$. Presented in the form $(R_H, R_{VC}, \alpha_C, \sigma_C)$ for T_S it appears at (3052.00, −2617.14, 2.44, 0) and for L_{O1} at (3052.00, −2617.14, 1.75, 19.54). The region below the curves is stable.

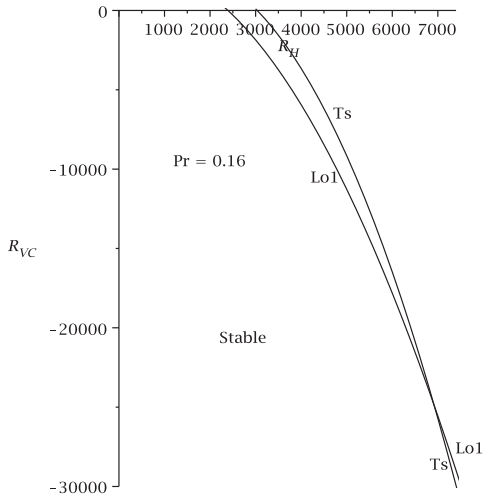

Fig. 3. Graphs of R_{VC} vs R_H for $Pr = 0.16$. New codimension-two point between Ts and L_{O1} for $R_V < 0$. Presented in the form $(R_H, R_{VC}, \alpha_C, \sigma_C)$ for T_S it appears at (6919.00, −24885.04, 2.38, 0) and for L_{O1} at (6919.00, −24885.38, 1.09, 31.66). The region below the curves is stable.

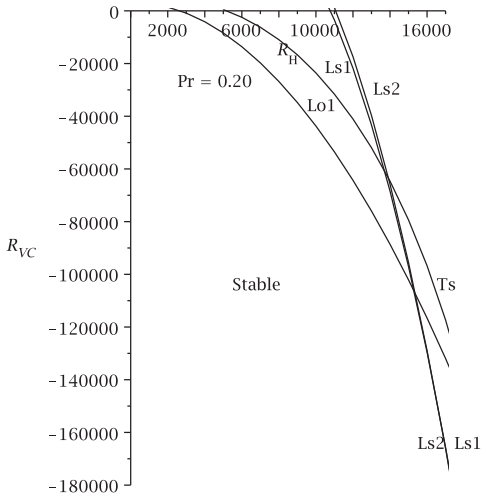

Fig. 4. Graphs of R_{VC} vs R_H for $Pr = 0.2$. New codimension-two point between L_{O1} and L_{S1} for $R_V < 0$. Then, L_{S1} and L_{S2} intersect again. Presented in the form $(R_H, R_{VC}, \alpha_C, \sigma_C)$, the new codimension-two point between L_{O1} and L_{S1} is at (15290.9, −106232.46, 0.58, 41.28) and (15290.9, −106232.46, 7.77, 0), respectively, and the second intersection between L_{S1} and L_{S2} is at (16725, −155536.86, 7.70, 0) and (16725, −155536.86, 7.77, 0), respectively. The region below the curves is stable.

2296.14, 2.80, 0) and for L_{O1} at (1178.00, 2296.77, 2.52, 9.41). The second new one appears for T_S at (6919.00, −24885.04, 2.38, 0) and for L_{O1} at (6919.00, −24885.38, 1.09, 31.66). The critical wave numbers of the two modes are a decreasing function of R_H and the critical frequency of oscillation of L_{O1} increases with R_H. Again the first and second longitudinal modes L_{S1} and L_{S2} are far away and are not relevant in this figure.

It is interesting to observe in Fig. 2 of [24] for $Pr = 0.2$, that these two modes already separate in such a way that apparently they are not able to intersect again for any negative R_V. Therefore, it is of interest to investigate here what happens when $Pr = 0.2$. In fact, due to the increase of R_{VC} in the curve of T_S [24], a new unexpected codimension-two point is found for negative R_V. As shown in Fig. 4, now the first longitudinal oscillatory mode L_{O1} first intersects the first longitudinal stationary mode L_{S1} when $R_H = 15290.9$ and $R_{VC} = -106232.46$. These two modes are even forming one convection cell. This concept comes from the analytical solutions of natural convection [17] which in the absence of shear ($R_H = 0$) present symmetry with respect to the origin forming one cell. The symmetry is best seen in the second even mode ($R_H = 0$) which presents three cells where the two close to the walls rotate in the same direction. This mode is very stable in the absence of shear but becomes mode L_{S1} when $R_H > 0$ [25]. After the codimension-two point the mode L_{S1} is the first unstable one. Nevertheless, for a further increase of R_H, numerical results demonstrate that modes L_{S1} and the second longitudinal stationary mode L_{S2} are able to intersect again for $R_H = 16725$ and $R_{VC} = -155536.86$. Their first intersection is irrelevant for $Pr = 0.2$, but it is important only for $Pr > 0.5$ (strict inequality, see [24,25]). In this way, the stability panorama changes in a relevant way when R_{VC} is negative.

The second odd longitudinal mode L_{S2} also appears from the odd mode of natural convection [17] in the absence of shear ($R_H = 0$). This mode is very stable with a very large critical R_V. It stabilizes further with R_H and, after a certain point with $R_{VC} > 0$, its critical curve decreases very fast to become relevant for $R_{VC} < 0$. The odd mode L_{S2} shows two anti-symmetric convection cells rotating in different directions [25].

Written in the form $(R_H, R_{VC}, \alpha_C, \sigma_C)$ the first codimension-two point between T_S and L_{O1} is at (1008, 2652.39, 2.88, 0) and (1008, 2652.39, 2.62, 8.55), respectively. The new codimension-two point between L_{O1} and L_{S1} is located at (15290.9, −106232.46, 0.58, 41.28) and (15290.9, −106232.46, 7.77, 0), respectively. The second intersection between L_{S1} and L_{S2} is found at (16725, −155536.86, 7.70,0) and (16725, −155536.86, 7.77,0). Clearly, the last two intersections have negative R_{VC}. At the codimension-two point, the one-cell structure of the first longitudinal oscillatory (even) mode L_{O1} changes into the three-cell structure of the first longitudinal stationary (even) mode L_{S1} [24,25]. However, the cooling from below and the increase of shear by R_H transforms the pattern into the two-cell structure of the second longitudinal stationary (odd) mode L_{S2}. Note that when $Pr = 0.2$ the oblique oscillatory Ob_O mode is still not able to appear for any R_H.

This magnitude of $R_{VC} = -106232.46$ at the intersection between L_{O1} and L_{S1} is very large. However, the tendency of the magnitude of R_{VC} in the curve L_{O1} is to increase to positive magnitudes with Pr, as can be seen in the next Fig. 5. Note that the R_{VC} of mode T_S increases faster. The importance of this intersection only persists until the appearance of the new oblique oscillatory mode Ob_O, event which occurs somewhere in the range $0.2 \leqslant Pr \leqslant 0.45$ (see Fig. 5). The critical wave number of L_{O1} decreases monotonically with R_H and those of L_{S1} and L_{S2} change slowly below and above a value of 8, respectively. The critical frequency of L_{O1} increases monotonically with R_H.

When $Pr = 0.45$, it is shown in Fig. 4 of [24] that the new oblique oscillatory mode Ob_O is already present. It is interesting that Ob_O is the first unstable one (below L_{O1}) when the angle of propagation of the perturbation is $\phi = 86^\circ$ and (8300, 1582.34, 1.4, 60.38). As shown in [24], Ob_O intersects L_{S1} when $Pr = 0.4886$ and $R_{VC} = 0$ (see Fig. 4(b) of [24]). However, it is demonstrated in Fig. 5 for $Pr = 0.45$ that the one-cell oblique oscillatory mode Ob_O and the three-cell even longitudinal stationary mode L_{S1} intersect in a new codimension-two point for $R_V < 0$. After the intersection the first unstable mode is L_{S1}. The full picture now may be described as follows. Presented in the form $(R_H, R_{VC}, \alpha_C, \sigma_C)$, the first codimension two point appears at (1105.00,3588.98,2.88,0) for T_S and at (1105,3587.95,2.71,10.43) for L_{O1}.

The second new codimension two point is located at (12637.95,-5655.59,8.17,0) for L_{S1} and at (12637.95,-5655.79,1.59, 108.79) with $\phi = 67^\circ$ for Ob_O. In addition, the even three-cell mode L_{S1} and the odd two-cell mode L_{S2} intersect again at the points (18627, −135181.5, 8.48, 0) for L_{S1} and (18627, −135181.5, 8.55, 0) for L_{S2}. After that point, L_{S2} is the first unstable mode. Evidently, the magnitude of the negative Rayleigh number at the

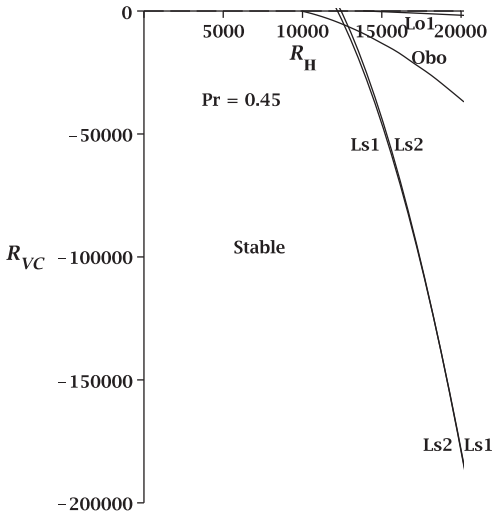

Fig. 5. Graphs of R_{VC} vs R_H for $Pr = 0.45$. New codimension-two point between Ob_O and L_{S1} for $R_V < 0$. Then, L_{S1} and L_{S2} intersect again. Presented in the form $(R_H, R_{VC}, \alpha_C, \sigma_C)$, the new codimension-two point between Ob_O and L_{S1} is at (12637.95, −5655.69, 8.17, 0) for L_{S1} and at (12637.95, −5655.69, 1.59, 108.79) and $\phi = 67°$ for Ob_O. The second intersection between L_{S1} and L_{S2} is at (18627, −135181.5, 8.48, 0) and (18627, −135181.5, 8.55, 0), respectively. The region below the curves is stable.

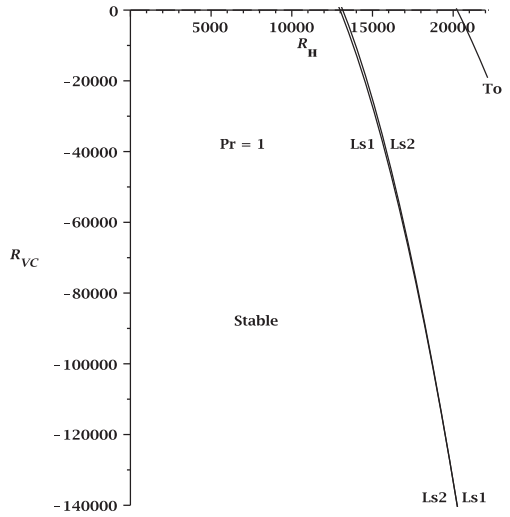

Fig. 6. Graphs of R_{VC} vs R_H for $Pr = 1$. Presented in the form $(R_H, R_{VC}, \alpha_C, \sigma_C)$, the new intersection point between L_{S1} and L_{S2} occurs at (19975, −132766.15, 9.14, 0) for L_{S1} and (19975, −132766.15, 9.18, 0) for L_{S2}. The region below the curves is stable.

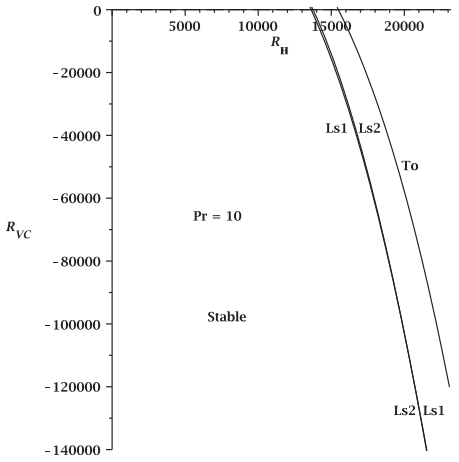

Fig. 7. Graphs of R_{VC} vs R_H for $Pr = 10$. Presented in the form $(R_H, R_{VC}, \alpha_C, \sigma_C)$, the new intersection point between L_{S1} and L_{S2} occurs at (20757, −120860.80, 9.79,0) for L_{S1} and (20757, −120860.80, 9.81,0) for L_{S2}. The region below the curves is stable.

intersection is smaller with respect to that of $Pr = 0.2$. The wavenumbers of the oblique oscillatory mode are almost constant for negative R_V. Those of L_{S1} and L_{S2} are below and above 8, respectively. However, the frequency of oscillation of Ob_O increases with R_H faster than that of L_{O1}. The angle of propagation of the perturbation decreases with R_H but the slope is less steep for $R_V < 0$.

The results presented above correspond to Prandtl numbers smaller than one. Here, the Prandtl number is one or larger than one as investigated in Refs. [24,25]. Those papers show the important competition between the stationary modes L_{S1} and L_{S2}. They cover a very large instability region with respect to R_H. Mode L_{S1} is the first unstable one for relatively small R_H. Then, the transversal oscillatory mode T_O is the first unstable one in a very short range. For larger magnitudes of R_H the mode L_{S2} is the first unstable one up to an intersection point after which L_{S1} becomes the first unstable one. For a further increase of R_H, those curves touch the axis $R_{VC} = 0$ with L_{S1} as the first unstable one. From this stability picture, it is clear that only the stationary modes L_{S1} and L_{S2} are able to be the first unstable ones for $R_V < 0$.

In order to check what happens with these modes, a first test is made using the approximate analytical formulas for L_{S1} and L_{S2} presented in Appendix A of [25]. Those formulas are very accurate for $Pr \geqslant 10$. According to the numerical results, both curves L_{S1} and L_{S2} intersect each other again for negative R_V. Consequently, mode L_{S2} can become the first unstable one for a second time. These results have been confirmed by means of a higher order Galerkin algorithm and are shown in Figs. 6–8 where $Pr = 1$, 10 and 100, respectively.

When presented in the form $(R_H, R_{VC}, \alpha_C, \sigma_C)$, the new intersection points between L_{S1} and L_{S2} occur for $Pr = 1$ at (19975, −132766.15, 9.14, 0) for L_{S1} and (19975, −132766.15, 9.18, 0) for L_{S2}, for $Pr = 10$ at (20757, −120860.80, 9.79, 0) for L_{S1} and (20757, −120860.80, 9.81, 0) for L_{S2} and for $Pr = 100$ at (20825.87, −119354.52, 9.86, 0) for L_{S1} and (20825.87, −119354.52, 9.88, 0) for L_{S2}. Notice that the magnitudes of the negative R_{VC} decrease even more with Pr in comparison with the previous Prandtl numbers ($Pr < 1$) used. It is important to stress again that the results of the approximate analytical formulas of Ref. [25] are valid for $Pr \geqslant 10$ and that consequently their numerical results lead to the conclusion that the second intersection between L_{S1} and L_{S2} occurs for all $Pr \geqslant 10$ when $R_{VC} < 0$. The wavenumbers of L_{S1} and L_{S2} increase monotonically with R_H and their magnitudes are very similar.

3.1. Importance of the main temperature profile

According to the results presented above, the flow still presents instabilities and changes of modes even under a negative vertical temperature gradient. The question arises about the possibility of a complete stabilization in the presence of a horizontal temperature gradient. This is a difficult question because the shear flow due to R_H is still present and is able to produce flow instabilities. Note that only the z-dependent part of the temperature profile is considered. That is

$$T(z) = R_H^2\left(\frac{7z}{5760} - \frac{z^3}{144} + \frac{z^5}{120}\right) - R_V z. \tag{15}$$

The roots of the first derivative of $T(z)$ with respect to z, give the location of the maximum and the minimum of the temperature.

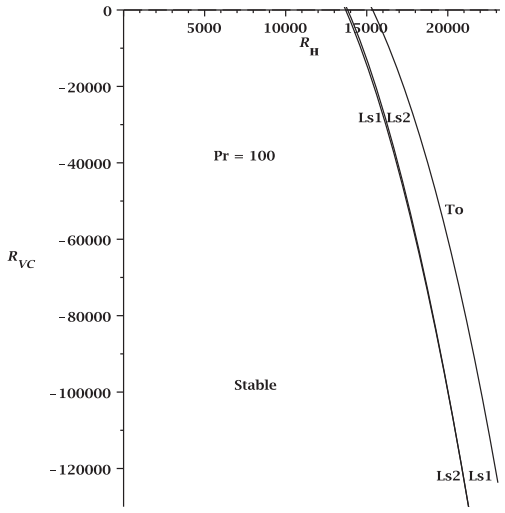

Fig. 8. Graphs of R_{VC} vs R_H for $Pr = 100$. Presented in the form $(R_H, R_{VC}, \alpha_C, \sigma_C)$, the new intersection point between L_{S1} and L_{S2} occurs at (20825.87, −119354.52, 9.86,0) for L_{S1} and (20825.87, −119354.52, 9.88,0) for L_{S2}. The region below the curves is stable.

They are responsible for the existence of the two unstable regions near to the walls and the stable region in between (see [24,25]). Their locations are at:

$$z_{max,min} = \pm\frac{1}{2}\sqrt{1-\frac{2}{15}\sqrt{30+21600\frac{R_V}{R_H^2}}} \tag{16}$$

Notice that the roots with a plus sign inside the first square root are outside the range of the walls and have no importance here. The three roots $z = 0$, 1/2 and −1/2 of the second derivative are the locations of the inflection points of the temperature profile. Substitution of Eq. 16 into the second derivative shows that the root with the plus sign corresponds to a minimum and that of the minus sign to a maximum. Observe that both roots approach to the walls locations $z = \pm 1/2$ increasing the negative magnitude of R_V in the term $30–21600\ |R_V|/R_H^2$. Accordingly, the negative R_V has a stabilizing effect by reducing the thickness of the unstable regions near to the walls. As can be seen from the results presented above, even at large magnitudes of negative R_V the system still admits convective instabilities. Therefore, the magnitude of the negative R_V has to be extremely large to have a complete stabilizing effect. It is difficult to tell after which thickness of the unstable regions the flow is already stable. Nevertheless, it is reasonable to assume that the flow is stable when the unstable regions completely disappear from the temperature profile. This condition is attained when the extrema of the temperature profile are located just at the walls (at $z_{max,min} = \pm 1/2$), that is, when the magnitude of the negative R_V with respect to R_H is a root of the radicand of Eq. (16). That is

$$R_V = -\frac{R_H^2}{720}. \tag{17}$$

This is in contrast with the results of $R_V > 0$ [24,25] where the temperature profile loses the stable region and transforms into a monotonically decreasing function of z when R_V increases for a fixed R_H.

The strong increase of the stable region with $R_V < 0$ in the temperature profile produces, as a consequence, the change of the three-cell even convection mode L_{S1} into the two-cell odd convection mode L_{S2} in a wide range of the Prandtl number.

4. Conclusions

In this paper the stability of a liquid layer subjected to an inclined temperature gradient is investigated under the action of a negative R_V. The goal is to present results which cover the full range of magnitudes of the Prandtl number investigated in the two previous papers [24,25]. Seven sample Prandtl numbers are used, $Pr = 0.14$, 0.16, 0.2, 0.45, 1,10 and 100.

It is interesting to note that two codimension-two points between T_S and L_{O1} start to appear around $Pr = 0.14$, one for positive R_V [24] and another new one for negative R_V. This Prandtl number is nearly the critical one after which these new phenomena occur. Calculations are done too for $Pr = 0.16$ in order to determine how large is the change of the negative R_V to reach a codimension-two point with an small increase of Pr. It is found that a very large magnitude of $R_V < 0$ is still able to change the stability of the fluid layer by means of a codimension-two point.

For a small increase of the Prandtl number up to $Pr = 0.2$, a new codimension-two point is found between the even longitudinal oscillatory mode L_{O1} and the even longitudinal stationary mode L_{S1} for $R_V < 0$. The magnitude of the negative vertical Rayleigh number of the codimension-two point decreases with a further increase of the Prandtl number. This point persists up to the first Prandtl number where the oblique oscillatory mode appears.

The interest focused next on the behavior of the oblique oscillatory mode Ob_O. The numerical results show that for $R_V < 0$ it is possible to find a codimension-two point between Ob_O and L_{S1} for smaller Prandtl numbers than $Pr = 0.4886$, which was thought to be the first one to show this point (see Fig. 4(b) in [24]). An example for $Pr = 0.45$ is presented where the curves Ob_O and L_{S1} intersect in a codimension-two point with $R_{VC} = -5655.69$. This codimension-two point disappears decreasing the Prandtl number to a magnitude where Ob_O vanishes.

As can be understood from [24,25], only two modes qualify to give interesting results for $Pr \geqslant 0.2$ and $R_V < 0$. They are L_{S1} (even mode, symmetric with three cells) and L_{S2} (odd mode, antisymmetric with two cells) (see [25]). For simplicity, first use is made of the analytical formulas of Appendix A in Ref. [25] valid for $Pr \geqslant 10$. Numerical calculations show that modes L_{S1} and L_{S2} intersect again for $R_V < 0$. This is verified with a higher order Galerkin numerical analysis for $Pr = 1$, 10 and 100. The magnitude of the negative R_V of the intersection point is large but decreases with Pr. After the intersection the mode L_{S2} is able to be the first unstable one for a second time. Accordingly, the analytical formulas [25] predict that this new intersection between L_{S1} and L_{S2} appears for all $Pr \geqslant 10$ and $R_V < 0$.

These results were a motivation to find out if these two curves also intersect for smaller Prandtl numbers. It is found that when $R_V < 0$, these two curves are relevant and also intersect at $Pr = 0.2$. Numerical calculations show that, in comparison with large Prandtl numbers, for this small Pr the magnitude of $R_V < 0$ at the crossing point increases and that of R_H decreases. Finally, it is concluded that for negative R_V the curves L_{S1} and L_{S2} always intersect for $Pr \geqslant 0.2$. After that intersection point, invariably the mode L_{S2} becomes the first unstable one.

The results presented above give a more complete picture of the linear natural convection of an infinitely large fluid layer under an inclined temperature gradient. It is concluded that, even in the case of $R_V < 0$, flow instabilities are still present and that it is always possible to find interesting flow patterns.

Conflict of interest

We wish to confirm that there are no known conflicts of interest associated with this publication and there has been no significant financial support for this work that could have influenced its outcome.

Acknowledgments

The authors would like to thank Joaquín Morales, Caín González, Alberto López, Raúl Reyes, Ma. Teresa Vázquez and Oralia Jiménez for technical support. A. S. Ortiz-Pérez would like to thank Juan de Dios Ocampo Diaz from Universidad Autónoma de Baja California and José Luis Guerrero Cervantes from CECyT No. 9, IPN for technical support.

References

[1] D.T.J. Hurle, E. Jakeman, C.P. Johnson, Convective temperature oscillations in molten gallium, J. Fluid Mech. 64 (1974) 565–576.
[2] A.E. Gill, A theory of thermal oscillations in liquid metals, J. Fluid Mech. 64 (1974) 577–588.
[3] J.E. Hart, Stability of thin non-rotating hadley circulations, J. Atmos. Sci. 29 (1972) 687–697.
[4] M. Lappa, Secondary and oscillatory gravitational instabilities in canonical three-dimensional models of crystal growth from the melt. II: lateral heating and the Hadley circulation, C.R. Mec. 335 (2007) 261–268.
[5] H.P. Kuo, S.A. Korpela, A. Chait, P. Marcus, Stability of natural convection in a shallow cavity, in: Proceedings of the 8th International Heat Transfer Conference, vol. 4, 1986, pp. 1539–1544.
[6] H.P. Kuo, S.A. Korpela, Stability and finite amplitude natural convection in a shallow cavity with insulated top and bottom and heated from a side, Phys. Fluids 31 (1988) 33–42.
[7] T.-M. Wang, S.A. Korpela, Convection rolls in a shallow cavity heated from the side, Phys. Fluids A 1 (1989) 947–953.
[8] P. Laure, Study of convective motions in a rectangular cavity with horizontal gradient of temperature, J. Theor. Appl. Mech. 6 (1987) 351–382.
[9] P. Laure, B. Roux, Linear and non-linear analysis of the hadley circulation, J. Cryst. Growth 97 (1989) 226–234.
[10] G.O. Hughes, R.W. Griffiths, Horizontal convection, Annu. Rev. Fluid Mech. 40 (2008) 185.
[11] A.Yu. Gelfgat, P.Z. Bar-Yoseph, A.L. Yarin, Stability of multiple steady states of convection in laterally heated cavities, J. Fluid Mech. 388 (1999) 315–334.
[12] M.C. Hung, C.D. Andereck, Transitions in convection driven by a horizontal temperature gradient, Phys. Lett. A 132 (1988) 253–258.
[13] W. Wang, R.X. Huang, An experimental study on thermal circulation driven by horizontal differential heating, J. Fluid Mech. 540 (2005) 49–73.
[14] I. Baaziz, N. Ben Salah, S. Kaddeche, Magnetic control of natural convection in the horizontal Bridgman configuration using a spectral method: transversal plan, Int. J. Comput. Fluid Dyn. 28 (2014) 339–350.
[15] M. Lappa, Thermal Convection, John Wiley & Sons, London, 2010.
[16] M. Lappa, Rotating thermal flows in natural and industrial processes, John Wiley & Sons, Chichester, 2012.
[17] S. Chandrasekhar, Hydrodynamic and Hydromagnetic Stability, Dover Publications Inc, New York, 1981.
[18] J.E. Weber, On thermal convection between non-uniformly heated planes, Int. Heat Mass Transfer 16 (1973) 961–970.
[19] D. Sweet, E. Jakeman, D.T.J. Hurle, Free convection in the presence of both vertical and horizontal temperature gradients, Phys. Fluids 20 (1977) 1412–1415.
[20] S.P. Bhattacharyya, S. Nador, Stability of thermal convection between non-uniformly heated plates, Appl. Sci. Res. 32 (1976) 555–570.
[21] J.E. Weber, On the stability of thermally driven shear flow heated from below, J. Fluid Mech. 87 (1978) 65–84.
[22] D.A. Nield, Convection induced by an inclined temperature gradient in a shallow horizontal layer, Int. J. Heat Fluid Flow 15 (1994) 157–162.
[23] P.N. Kaloni, N. Qiao, On the nonlinear stability of thermally driven shear flow heated from below, Phys. Fluids 8 (1996) 639–641.
[24] A.S. Ortiz-Pérez, L.A. Dávalos-Orozco, Convection in a horizontal fluid layer under an inclined temperature gradient, Phys. Fluids 23 (2011) 084107.
[25] A.S. Ortiz-Pérez, L.A. Dávalos-Orozco, Convection in a horizontal fluid layer under an inclined temperature gradient for Prandtl numbers Pr 1, Int. J. Heat Mass Transfer 68 (2014) 444–455.
[26] M. Lappa, Exact solutions for thermal problems: Buoyancy, Marangoni, vibrational and magnetic-field-controlled flows, Rev. Appl. Phys. 1 (2012) 1–14.
[27] V.K. Andreev, I.V. Stepanova, Ostroumov–Birikh solution of convection equations with nonlinear buoyancy force, Appl. Math. Comput. 228 (2014) 59–67.
[28] B.A. Finlayson, The Galerkin method applied to convective instability problems, J. Fluid Mech. 17 (1968) 201–208.
[29] B.A. Finlayson, The Method of Weighted Residuals and Variational Principles, Mathematics in Science and Engineering, Academic Press, New York, USA, 1972.
[30] J.E. Hart, A note of stability of low-Prandtl-number Hadley circulations, J. Fluid Mech. 132 (1983) 271–281.
[31] D. Ceotto, Thermal diffusivity, viscosity and Prandtl number for molten iron and low carbon steel, High Temp. 51 (2013) 131–134.